



## **Realizing a 140 GHz Gap Waveguide–Based Array Antenna by Low-Cost Injection Molding and Micromachining**

Downloaded from: <https://research.chalmers.se>, 2023-05-05 01:15 UTC

Citation for the original published paper (version of record):

Farjana, S., Ghaderi, M., Uz Zaman, A. et al (2021). Realizing a 140 GHz Gap Waveguide–Based Array Antenna by Low-Cost Injection Molding and Micromachining. *Journal of Infrared, Millimeter, and Terahertz Waves*, 42(8): 893-914.  
<http://dx.doi.org/10.1007/s10762-021-00812-8>

N.B. When citing this work, cite the original published paper.



# Realizing a 140 GHz Gap Waveguide–Based Array Antenna by Low-Cost Injection Molding and Micromachining

Sadia Farjana<sup>1</sup> · Mohammadmir Ghaderi<sup>1</sup> · Ashraf Uz Zaman<sup>2</sup> · Sofia Rahiminejad<sup>3</sup> · Thomas Eriksson<sup>2</sup> · Jonas Hansson<sup>4</sup> · Yinggang Li<sup>5</sup> · Thomas Emanuelsson<sup>6</sup> · Sjoerd Haasl<sup>7</sup> · Per Lundgren<sup>1</sup> · Peter Enoksson<sup>1</sup>

Received: 27 November 2020 / Accepted: 26 August 2021  
© The Author(s) 2021

## Abstract

This paper presents a novel micromachining process to fabricate a 140 GHz planar antenna based on gap waveguide technology to be used in the next-generation backhauling links. The 140 GHz planar array antenna consists of three layers, all of which have been fabricated using polymer-based microfabrication and injection molding. The 140 GHz antenna has the potential to be used as an element in a bigger 3D array in a line-of-sight (LOS) multiple input multiple output (MIMO) configuration to boost the network capacity. In this work, we focus on the fabrication of a single antenna array element based on gap waveguide technology. Depending on the complexity of each antenna layer's design, three different micromachining techniques, SU8 fabrication, polydimethylsiloxane (PDMS) molding, and injection molding of the polymer (OSTEMER), together with gold (Au) coating, have been utilized to fabricate a single 140 GHz planar array antenna. The input reflection coefficient was measured to be below  $-11$  dB over a 14% bandwidth from 132 to 152 GHz, and the antenna gain was measured to be 31 dBi at 140 GHz, both of which are in good agreement with the simulations.

**Keywords** Gap waveguide · Injection molding · LOS-MIMO · OSTEMER · Planar antenna · PDMS · SU8 · Slot array

## 1 Introduction

With the development of future 5G networks, point-to-point backhauling links that connect several base stations within the wireless network will play a very critical role in overall network performance. In 5G, data traffic will grow enormously ( $\sim 50$  Gbps) at the base stations, where each user will have more than 1 Gbps data

---

✉ Sadia Farjana  
farjana@chalmers.se

Extended author information available on the last page of the article



**Fig. 1** Ericsson demonstrator of LOS-MIMO at 70 GHz band [5]

connectivity. Today's microwave backhaul link will not be able to handle this massive data traffic. To make this possible, research on the use of frequencies beyond 100 GHz, targeting the support of the 5G evolution, is now in progress [1, 2].

Even though frequencies above 100 GHz are considered for next-generation backhauling systems, it will be challenging to provide data rates above 50 Gbps over a large distance using a single point-to-point link due to high path-loss and limited output power from the available active circuits above 100 GHz. To overcome this issue, researchers have proposed new enabler technologies such as the line-of-sight (LOS) multiple input multiple output (MIMO) concept where an array of antennas with specific spatial separation is used to support several independent channels between the transmitter (TX) and the receiver (RX) [3, 4]. The LOS-MIMO concept has been tested recently between 70 and 80 GHz by the telecom operators [5]. An example of a LOS-MIMO array is shown in Fig. 1. The LOS-MIMO systems are different than the conventional single antenna point-to-point backhauling systems. Interestingly enough, it can be shown that the link budget for a  $M \times M$  LOS-MIMO link is  $10\log_{10}M$  dB better than the corresponding link budget for  $M$  parallel and independent SISO links. For example, a 16 TX, 16 RX LOS-MIMO link has a signal-to-noise ratio (SNR) that is 12 dB better than a corresponding link with 16 parallel SISO channels (also with 16 TX, 16 RX antennas, but with no cross talk) with the same conditions otherwise. This fact makes LOS-MIMO links attractive at high frequencies, where power is difficult to generate. However, there exist no specific *European Telecommunications Standards Institute (ETSI)* side lobe standards for such an array antenna at the moment.

From the published literature on antennas above 100 GHz, we find that there is a big gap among available antenna technologies in terms of performance, fabrication complexity, and cost. The most common antennas above 100 GHz are horn-feed reflectors, microstrip patch arrays, and waveguide-based slot array antennas.

Although in these antennas the reflectors cover relatively large bandwidth, and in general have high efficiency, their form factors are not appropriate for LOS-MIMO array configuration [6]. The waveguide-based slot arrays have high efficiency, but the impedance bandwidth of the series-fed low complexity slot array is relatively small which makes it unfit for the LOS-MIMO application [7–9]. On the other hand, employing printed circuit board technologies such as liquid crystal polymer (LCP) or low-temperature co-fired ceramic (LTCC)-based arrays suffer from high dielectric losses and lower antenna efficiencies [10–12]. A planar antenna with high efficiency and gain with low fabrication complexity and low-cost production is preferable for commercial LOS-MIMO solutions.

Fabrication of antennas above 100 GHz is another challenge. Recent developments in CNC milling techniques have allowed fabrication of low-loss and high-gain waveguide-based antennas around 100–200 GHz frequency range [13, 14]. CNC is a widely used metal milling technique. However, CNC milling-based technique must use very small milling tools for achieving required dimensional features in a waveguide antenna array above 100 GHz. This consequently increases the required amount of machining time and does not allow low-cost mass-production of large waveguide antenna arrays. Diffusion bonding is another fabrication method which has been used for realizing high-efficiency waveguide-based antenna arrays [8, 15]. In this method, a hollow waveguide-based multi-layer structure is formed by stacking etched metal plates in vacuum at high temperature (around 1000 °C with precise thermal control) and high mechanical pressure. In this case, the required number of fabrication steps and prerequisite conditions lead to expensive serial manufacturing techniques, suitable only for high-end scientific instrumentation or special prototypes. Therefore, this technique is not feasible for low-cost mass-production of high-gain antenna arrays.

Apart from the abovementioned fabrication techniques, deep reactive ion etching (DRIE)-based silicon micromachining and SU8 polymer-based fabrication have been reported for high-frequency waveguide components and antenna systems [16, 17]. These are promising technologies for antenna fabrication at the sub-millimeter wave band. They allow precise fabrication and relatively low cost as compared to CNC milling or diffusion bonding techniques. Among these two methods, polymer-based thick layer SU8 photoresist technology affords good dimensional accuracy with low processing temperatures and at a relative low cost—making it a better choice for antenna manufacturing above 100 GHz. However, a wideband waveguide-based slot array needs multi-layer waveguide geometry and the SU8-based micromachining technique presents a shortcoming for this type of multi-layer geometry [17]. Despite many attractive features, the SU8 technique is a complicated fabrication process. Also, both DRIE-based silicon micromachining and SU8-based micromachining become expensive for antenna structures having a large aperture (more than 30 dBi gain) as very few antenna units can be placed on each wafer. Therefore, the cost of the antenna units cannot be reduced after a certain level.

Consequently, there is a need for new low-cost fabrication methods for fabricating waveguide-based antenna structures above 100 GHz. In this work, we propose a new fabrication method for fabricating a low-loss planar high-gain antenna above 100 GHz. Recently developed multi-layer gap waveguide technology has been

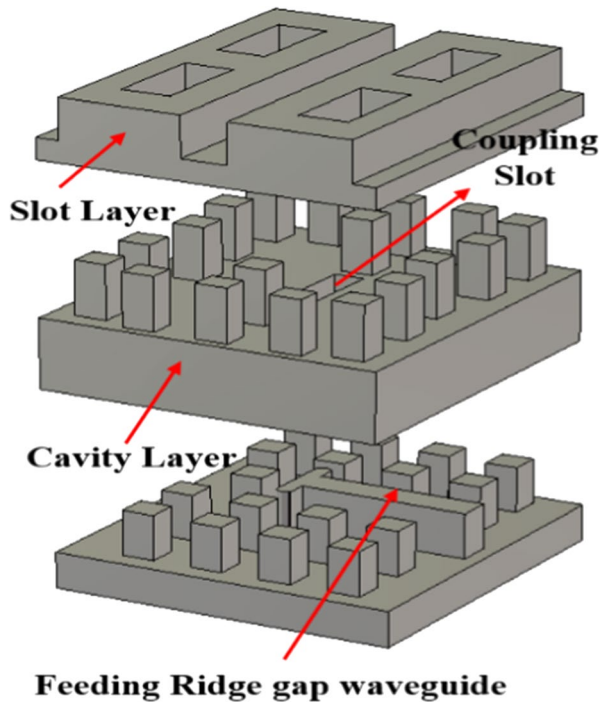
considered here due to the non-contact nature of this waveguide [18–20]. Previously, various gap waveguide components have been realized using silicon micromachining technology and SU8-based polymers [21, 22]. Here, we propose a low-cost polymer injection molding-based fabrication technique for realizing high-gain antennas at a 140 GHz frequency range. In the proposed method, a reusable polydimethylsiloxane (PDMS) mold tool is fabricated by using an SU8 master. Once this mold tool is fabricated, low-cost off-stoichiometry thiol-ene-epoxy polymer (OSTEMER) (Mercene Labs, Sweden) can be injected into the mold to realize different layers of the antenna. With the proposed approach, the cleanroom is only necessary to fabricate mold tools. The injection molding process and metallization of the molded parts can be performed effortlessly in a regular environment within a very short period. This will result in a high throughput of the devices, thereby reducing the cost significantly.

In our previous work, we used SU8 as a device material for one layer and master material for the two other layers [23]. Considering the challenges of SU8 fabrication and further investigation on PDMS molding lead us to modify the fabrication process. One of the major challenges of our previous process was the alignment challenge caused by the layers being made of different materials. In the current work, we present a new fabrication process where all layers are fabricated by injection molding of OSTEMER, a new type of thermosetting polymer developed specifically for microfabrication. The OSTEMER can be selected to provide a very stiff and flat surface. All materials and machining processes used here closely resemble the well-accepted standard soft lithography process resulting in a low-cost fabrication process [24]. This paper is organized as follows. Section 2 presents the design of a high-gain planar antenna based on gap waveguide technology. Section 3 presents the proposed MEMS fabrication technique, and Section 4 discloses the results, discussion, and comparison between already published and the presented work.

## 2 Design of the Planar Array

Gap waveguide technology can be explained as a metamaterial-based wave-guiding structure that uses a periodic electromagnetic band gap (EBG) geometry around a certain type of guiding path where electromagnetic waves can be guided and controlled even in an oversized parallel-plate structure [25]. This waveguide can be realized without any requirement of metal contact between the upper metal surface and the lower metal surface which is an advantage in the case of multi-layer waveguide structures, relaxing the fabrication tolerance requirements above 100 GHz. Moreover, gap waveguide-based slot arrays suffer neither from lossy dielectrics nor from unwanted radiation losses and these antennas operate at a relative bandwidth of more than 30% [26]. Usually, wideband waveguide slot arrays require corporate feed networks. Therefore, more space is required to design a feed network for such antenna array. Hence, an intermediate cavity layer is typically used between the radiating slot layer and the feeding waveguide layer. Figure 2 shows a subarray of the proposed antenna array with all three layers: the slot layer, the cavity layer, and the feeding layer.

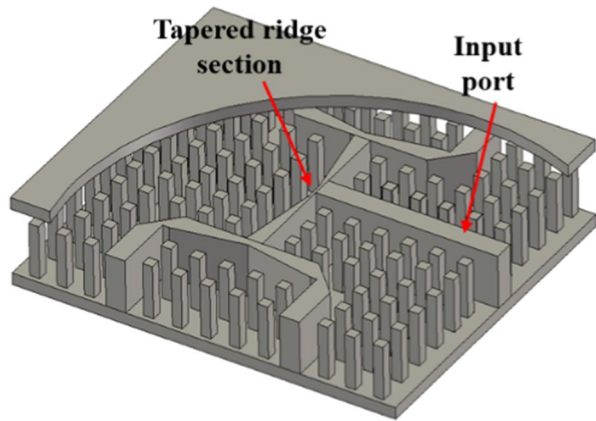
**Fig. 2** Exploded view of the multi-layer subarray concept



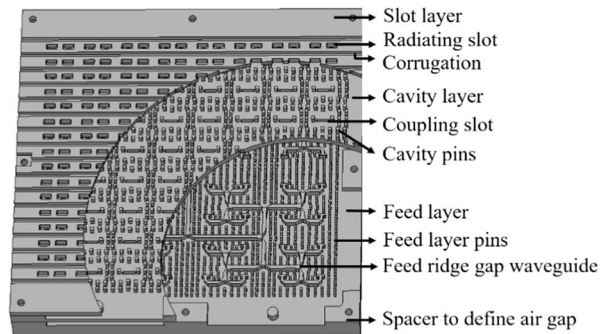
A complete  $16 \times 16$  slot array antenna consists of, in total, 64 such subarrays. The working principle of the proposed antenna is similar to the work mentioned in [27]. However, as some dimensions of the antenna were becoming very challenging to realize, this antenna has been re-optimized for the 140 GHz band, taking several fabrication limitations of the proposed fabrication method into consideration. As it is known from dual-layer cavity back slot arrays, here also the radiating slots are placed above the cavity layer. By proper design of the cavity, the four slots in each subarray can be excited with the same phase and amplitude, which is the key for broad side radiation. Also, a corrugation is added in the radiating layer to suppress the mutual coupling between the neighboring slot elements. The depth of these corrugations is optimized to improve both  $S_{11}$  and the radiation pattern of the antenna. The cavity layer is placed above the feeding layer and the electromagnetic energy is coupled from the feed layer to the cavity layer by the coupling slot placed at the bottom of the cavity layer. The feeding layer consists of sixty-three 3-dB power dividers cascaded one after another. One such section of 3-dB ridge gap power divider is shown in Fig. 3.

Figure 4a shows the geometric arrangement of the proposed multi-layer  $16 \times 16$ -element slot array antenna. A ridge gap waveguide power divider is built in a cascaded fashion to feed 64 cavities, each of which excites four radiating slots. The input section of the antenna is excited with a standard D-band (110–170 GHz) waveguide flange. Thus, a transition from normal rectangular waveguide to ridge gap waveguide is needed here. The transition used in this work is very similar to the

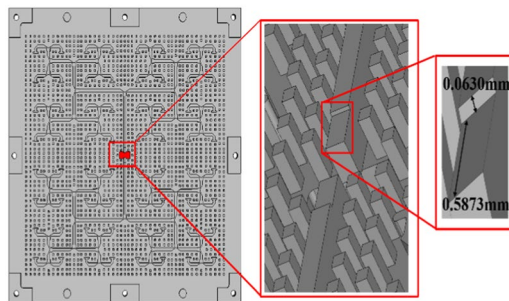
**Fig. 3** Three-dB power divider sections



**Fig. 4** **a** Numerical model of the proposed  $16 \times 16$ -element array antenna in CST microwave studio. **b** Transition from ridge gap waveguide to WR-6.5



(a)



(b)

symmetric transition proposed in [27]. A matching step at the end of each ridge is used to achieve a good matching from WR-6.5 to the ridge gap waveguide, shown in Fig. 4b. The pin dimensions in the cavity layer and the feed layer are designed according to the guidelines presented in [28] and are mentioned in Table 1. The complete antenna is simulated using CST microwave studio with open radiation boundaries. Figure 5 shows the simulated  $S_{11}$  of a  $2 \times 2$  subarray element, a complete



**Table 1** Parameters of the complete array antenna

Component	Parameter	Value (mm)
Radiating slot	Length	1.11
	Width	0.58
	Round radius	0.1
Distance between slot and cavity layer	Airgap	0.19
Corrugation	Width	0.47
	Depth	0.49
Top metal plate	Thickness	0.75
Coupling slot	Length	1.35
	Width	0.3
	Round radius	0.1
Cavity layer pin	Length	0.321
	Width	0.321
	Height	0.644
	Pin period	0.708
Middle metal plate	Thickness	1.39
Waveguide transition	Length of step	0.587
	Height of step	0.063
Bottom metal plate	Thickness	2.89
Feed ridge gap waveguide	Width	0.343
Feed layer pin	Length	0.214
	Width	0.214
	Height	0.644
	Period of pins	0.708
Aperture area	Length of the array	29.20
	Width of the array	26.4
Distance between feed and cavity layer	Air gap	0.19
Bottom waveguide opening	Length	1.63
	Width	0.815

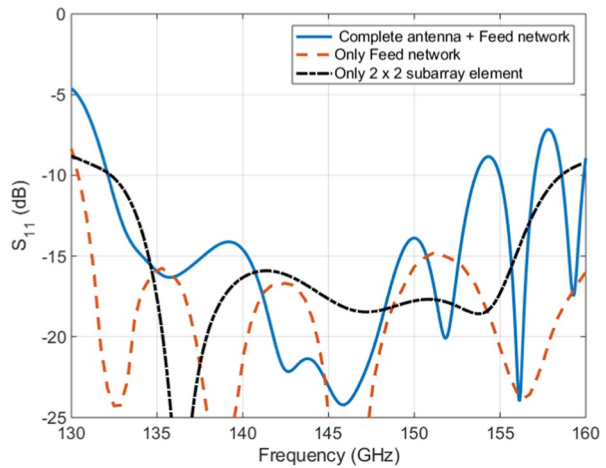
antenna array, and a stand-alone feed network, which is simulated by placing ports at each output of the 3-dB T-junction. Furthermore, Table 1 presents all important dimensions of the three layers of the complete antenna array.

### 3 Fabrication Process

To overcome the complications of conventional CNC machining, micromachining using a polymer was used to fabricate a gap waveguide-based slot array antenna operating at 140 GHz. SU8 is a negative photosensitive epoxy-based polymer. It is suitable to fabricate high-aspect ratio structures and can be spin-coated up to



**Fig. 5** Simulated  $S_{11}$  of the complete antenna array, the stand-alone feed network, and only  $2 \times 2$  subarray element



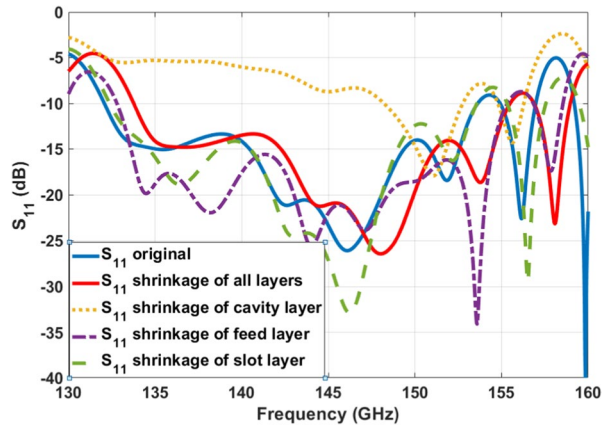
thicknesses of 1 mm in one layer. SU8 has previously been used for RF applications as well as for gap waveguide structures [17, 29–31].

Depending on the geometry of the proposed antenna and considering the challenges of SU8 fabrication, we reported a fabrication process where the slot layer of the proposed antenna design was fabricated with SU8 but the cavity layer and the feed layer were made of OSTEMER [23]. To fabricate the cavity layer and the feed layer, we used an SU8 master to produce the PDMS molds and later the PDMS molds were used for injection molding of OSTEMER. Further investigations of the fabrication process revealed that different layers made of different materials could cause misalignment between each layer due to a non-identical shrinkage rate of the polymers, which can affect the antenna performance. PDMS is known to shrink during curing [32, 33]. Even though OSTEMER does not shrink during curing, the shrinkage of the PDMS is transferred to the layers made of OSTEMER. SU8 on the other hand has a negligible shrinkage effect. Due to the PDMS shrinkage, we assume some misalignment will occur among the layers made of OSTEMER and the layer made out of SU8. Figure 6 shows the simulated  $S_{11}$  due to the abovementioned misalignment effect caused by the shrinkage of one individual layer at a time, and the simulation results when all layers have similar shrinkage compared to the design. Figure 6 clearly shows that if all the layers experience similar shrinkage, the mutual misalignment among layers will decrease and the overall antenna performance of the fabricated antenna will improve.

To avoid the complexity of using different materials for different layers and to make a more rapid process, we propose in this paper a new fabrication technique.

In this fabrication process, SU8 was only used to make master imprints for PDMS molds. An SU8 master was fabricated for each layer. These masters were in turn used to make PDMS molds for each layer. PDMS as a mold material offers several advantages such as high replication accuracy, reusability, and easy demolding [34]. The PDMS molds were used together with milled Al pieces for injection molding. The Al pieces defined the waveguide opening in the feed network layer and

**Fig. 6** Simulation results showing the shrinkage effect of a single layer and shrinkage effect when all layers experience similar shrinkage



the coupling slots in the groove gap cavity layer. The molds were then injected with the OSTEMER. The detailed fabrication process is described in this section. A schematic of the complete fabrication process is presented in Fig. 7.

### 3.1 SU8 Master Fabrication

The SU8 master consists of a SU8 base layer. For the base layer, SU8 2035 was dispensed on a 4" Si wafer, spun, baked, flood-exposed without a photomask, and then post-exposure baked. The rest of the fabrication process was optimized for each layer as described below.

#### 1) Slot layer master

To fabricate the slot layer master, SU8 2150 was dispensed on the base layer and spun to obtain a  $258 \mu\text{m} \pm 10 \mu\text{m}$  thick SU8 layer, followed by a typical soft baking process. The two-step soft baking that starts at  $65^\circ\text{C}$  and then ramped up to  $95^\circ\text{C}$  helps to decrease stress between the SU8 layer and the Si wafer. After that, the wafer was UV-exposed to outline the radiating slot elements and a post-exposure bake was done at  $75^\circ\text{C}$  for about 2 h. Once the first layer was done, SU8 2150 was dispensed, spun, and soft-baked on the previous layer to achieve an additional  $493 \mu\text{m} \pm 10 \mu\text{m}$  thick layer. After soft bake, the SU8 layer was UV-exposed to obtain the slots and the required corrugation between the two slots. Later, a post-exposure bake for 2 h was performed, and the wafer was subsequently developed with strong agitation in mr-Dev 600 solution to define the structures.

#### 2) Cavity layer master

Similarly, the cavity layer master also contained an SU8 base layer, pins, and the support spacer structure on the edge of the device. SU8 2150 was spun on the base layer to obtain a  $644 \mu\text{m} \pm 10 \mu\text{m}$  thick layer, followed by a soft bake, UV exposure, and a post-exposure bake. SU8 2035 was dispensed and spun on top of the previous  $644 \mu\text{m} \pm 10 \mu\text{m}$  thick layer to define the support spacers on the side of the structure. These support spacers help to maintain the needed air gap

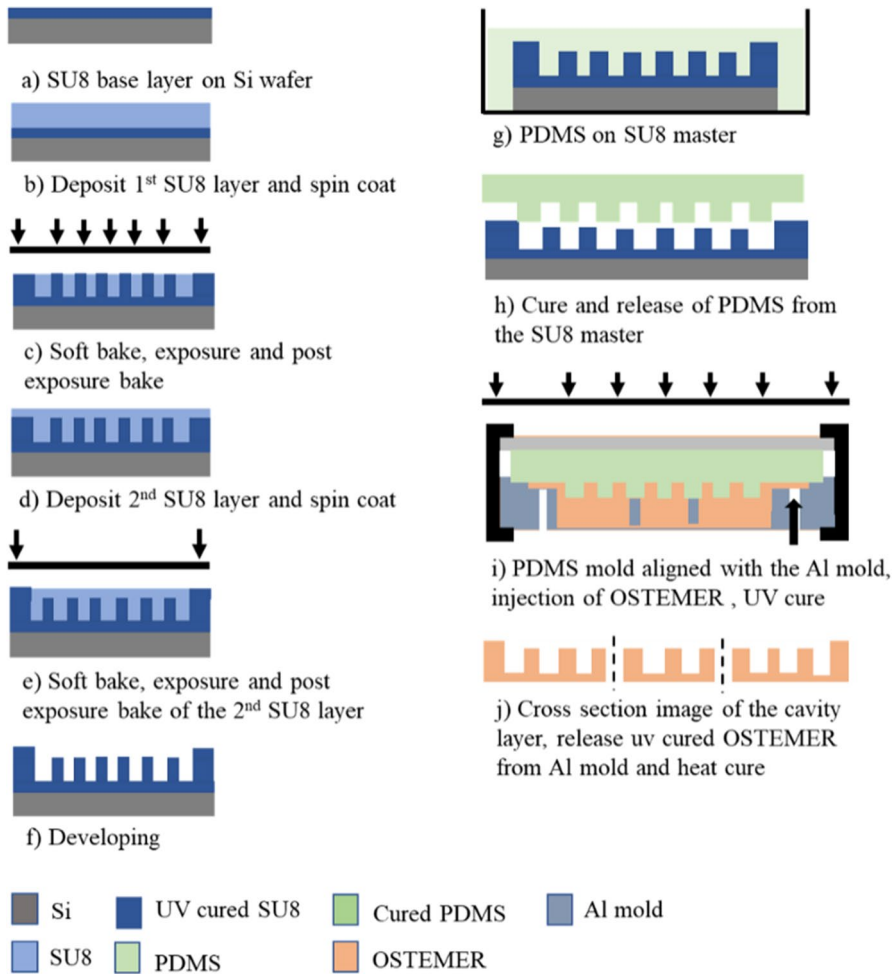


Fig. 7 Schematic of the complete fabrication process

between the top radiating layer and the cavity layer. Once soft bake, UV exposure, and post-exposure bake at 95 °C for 20 min were completed, SU8 layers were developed in mr-Dev 600 solution. Figure 7a–f show the process flow of fabricating the SU8 master for the cavity layer.

### 3) Feed layer master

The fabrication of the bottom feed layer SU8 master is similar to the fabrication process of the cavity layer master. An extra process step was added to make the small step in height on the ridge waveguide section at the opening of the bottom transition, as shown in Fig. 4b. To get a  $580\ \mu\text{m} \pm 10\ \mu\text{m}$  thick layer, SU8 2150

was again dispensed on the base layer and spun. Additional fabrication steps including soft bake, UV exposure, and post-exposure bake were also completed afterward. SU8 2035 was dispensed on top of thick SU8 2150 layer and spun to reach a thickness of  $63 \mu\text{m} \pm 1 \mu\text{m}$ , thus adding this layer to the periodic pins and defining the required height in the transition section. Later, the deposited layer was soft-baked and UV-exposed, followed by a post-exposure bake. SU8 2035 was dispensed again and spun to a thickness of  $110 \mu\text{m} \pm 1 \mu\text{m}$ , to define the spacers. After soft bake, UV exposure, and post-exposure bake, the wafer was developed in mr-Dev 600 solution.

After development, all the masters went through a hard baking process. The hard baking was done at  $150^\circ\text{C}$  for 20 min. The hard bake was done to strengthen the adhesion between the device structure and the base layer. The master was then treated with CHF<sub>3</sub> to make it non-stick and facilitate the release of the PDMS mold.

### 3.2 PDMS Molding

Sylgard 184 PDMS was used to make PDMS molds from all three SU8 masters. Obtaining PDMS molds for the cavity layer and the feed layer was relatively a straightforward process as there were no narrow openings. The PDMS was mixed in a standard 10:1 curing ratio, and the preparation time was less than 10 min. After pouring the PDMS prepolymer into the master, the PDMS was degassed in a vacuum chamber and later cured at  $80^\circ\text{C}$  for 3 h. The cured PDMS mold was removed from the master subsequently. For the slot layer, the SU8 master was dipped in a toluene bath for 2 min and dried with a nitrogen gun, before dispensing the PDMS. The toluene bath reduces the surface tension of the SU8 structure, hence allowing the high viscosity PDMS to enter the narrow slot openings. The PDMS was then degassed in a vacuum chamber, cured at  $80^\circ\text{C}$  for 3 h, and removed from the SU8 master. Figure 7g and h show the process flow of fabricating the PDMS mold from the SU8 master of the cavity layer.

### 3.3 Injection Molding

The PDMS molds were aligned with a milled aluminum (Al) mold which was used to define the waveguide opening in the feed network layer and the coupling slots in the groove gap cavity layer. The Al mold for the slot layer was flat as the complete structure was defined in the SU8 master and transferred to the PDMS mold. All Al molds have two holes, one for injecting OSTMER and one for extracting the air inside the cavity at the same time. The aligned Al mold and the PDMS mold were placed in a vacuum chamber before injecting with liquid OSTEMER 322 prepolymer. The OSTEMER prepolymer was exposed to UV through the transparent PDMS mold. The UV exposure initiates the polymerization of the liquid prepolymer and turned it into a solid but flexible OSTMER layer. The UV-cured OSTMER layer was then de-molded and hard-baked at  $120^\circ\text{C}$  for 2 h to obtain the mechanical stiffness. The hard-baked OSTMER layers were then sputtered with 20 nm thick titanium (Ti) and 200 nm thick Au and later electroplated with Au to achieve a conductive surface of  $1.1 \mu\text{m}$ . Figure 8 shows the injection molding setup.

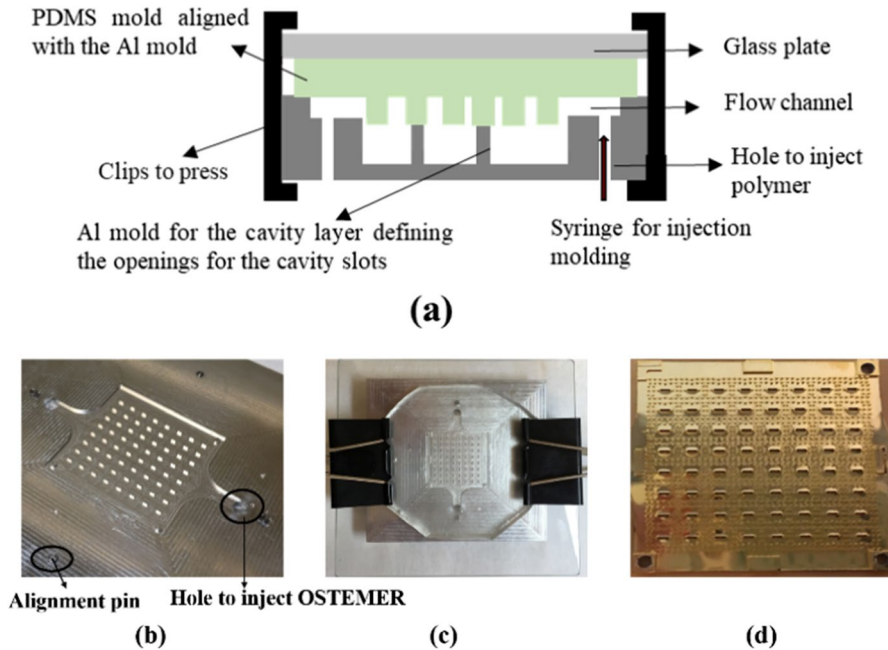


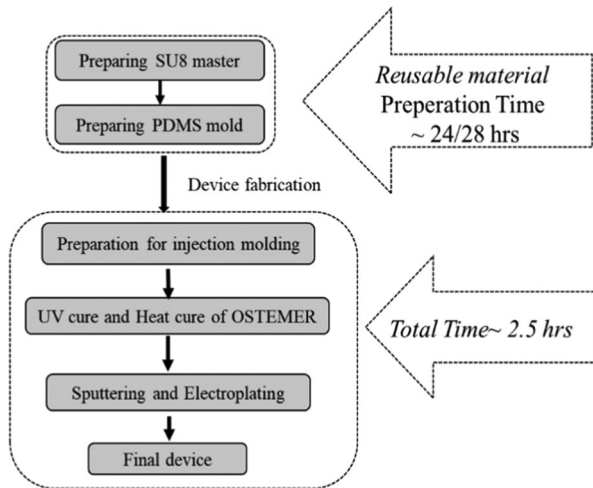
**Fig. 8** Injection molding setup for fabricating the cavity layer. **a** Schematic of injection molding setup. **b** Al mold with openings for coupling slots. **c** PDMS mold placed on Al mold for injection molding. **d** The cured and Au-coated OSTEMER cavity layer

### 3.4 Summary of Rapid Fabrication Process

The fabrication process described above states that the SU8 fabrication is the most extensive and complicated part of the complete fabrication process. The proposed template-based injection molding process overcomes the difficulties of SU8 fabrication, as the SU8 masters can be fabricated once and repeatedly used as a template. Furthermore, mass production of the antennas using OSTEMER injection molding can be performed without using the cleanroom facilities. As shown in Fig. 9, the time-consuming micromachining part and the complicated parts need to be prepared only once and can be reused later as templates. When the reusable part is prepared, the rest of the fabrication process can be carried out without the use of any cleanroom facility and is a comparatively fast and straightforward process.

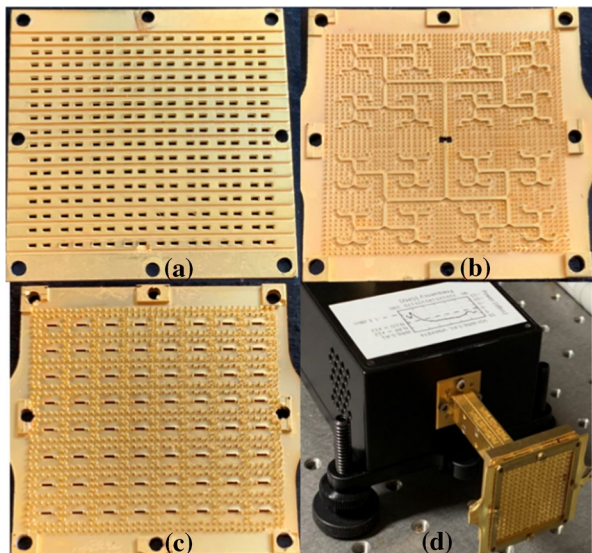
## 4 Measurement Results and Discussion

In this section, we present the measurement results of the antenna obtained from the adopted fabrication method, together with discussions of the results.

**Fig. 9** Flow chart of the fast fabrication process

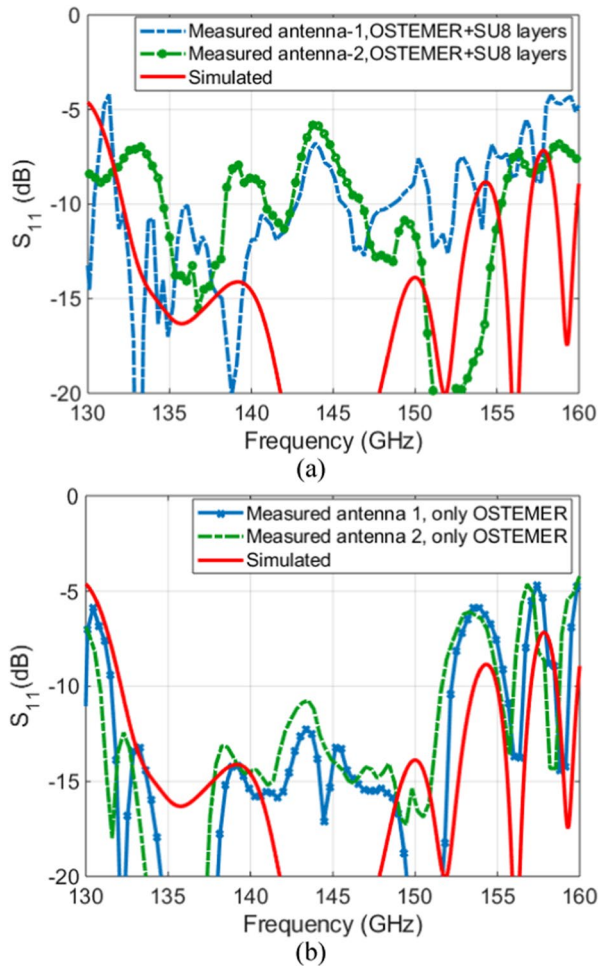
#### 4.1 Measurement Results of the Array Antenna

Figure 10 shows the fabricated parts and the assembled antenna. All the layers were fabricated using OSTEMER 322. The measurement was done using a Keysight PNA N5242A and VDI D-band extender module having a WR-6.5 waveguide interface. The simulated  $S_{11}$  for the complete  $16 \times 16$  element antenna array is well below  $-14$  dB level over the band of interest, 135–150 GHz (Fig. 5). Figure 11a presents the  $S_{11}$  measurement results of two antennas for the process where the slot layer was made of SU8 and the cavity and feed layers were made of OSTEMER. Figure 11b presents the measured  $S_{11}$  of two antennas where all the layers were made out of

**Fig. 10** Fabricated antenna. **a** Slot layer. **b** Feed layer. **c** Cavity layer. **d** Complete antenna module mounted with WR-6.5 flange



**Fig. 11** Simulated and measured  $S_{11}$  for the  $16 \times 16$  element antenna array. **a** Slot layer made of SU8, the cavity layer, and the feed layer made of OSTEMER. **b** All layers made of OSTEMER



OSTEMER. Two antennas were measured to assess the repeatability of the process and the measurements are compared to the simulation. Good agreement with the simulation result is observed and the measured  $S_{11}$  is below the  $-11$  dB level over the band of interest (Fig. 11b). Comparing Fig. 11a and b, we can see that the antenna's  $S_{11}$  performance has been improved over the band 132–152 GHz by changing the fabrication process. The improved  $S_{11}$  suggests that a reduction in the misalignment between layers improves the performance.

From the simulation results presented in Fig. 6, we see that the cavity layer is critical and shrinkage in the cavity layer has a detrimental effect on the performance of the antenna. This critical issue is explained below. For a specific resonance mode, magnetic field lines exist in two parts of the cavity as is shown in Fig. 12. These magnetic lines are cut by the radiating slots and, as a result, induce a perpendicular uniform electric field distribution in all the four radiating slots. The frequency



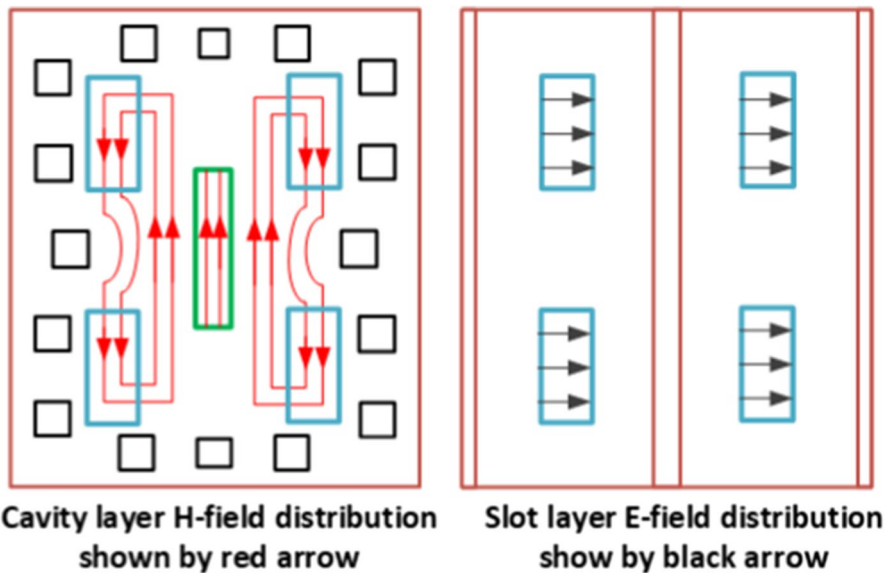


**Fig. 12** The magnetic field distribution (red lines) in the cavity layer and the electric field distribution in the slot layer (black lines) of the proposed antenna array

of the resonance mode inside the cavity layer and the resonance of the radiating slot antenna elements are usually optimized to have a maximum coupling of electromagnetic (EM) energy from the cavity layer to the slot layer. Dimensional variation in the cavity layer causes a change in frequency of the resonance mode and thus changes the magnetic field lines inside the cavity layer. This simultaneously causes a mismatch in resonance frequencies of the cavity layer and the slot layer. As a result, the EM energy is reflected to the feed layer (bottom layer of the antenna) instead of coupling to the slot layer, and the  $S_{11}$  of the antenna is greatly disturbed.

If we compare the measurement result of Fig. 11b with the simulated  $S_{11}$  result, we can see that the operating bandwidth has shifted slightly towards the lower frequencies. This shift is due to the inaccuracy in the compensation factor  $1.4 \pm 0.1\%$  of PDMS shrinkage in the layout design, which resulted in fabricated layers being slightly enlarged (approximately  $22 \mu\text{m}$  to  $32 \mu\text{m}$ ) compared to the target dimensions. Running full-wave simulations using different shrinkage values, we verified that the same shrinkage or expansion of all layers compared to the nominal dimensions will cause a bandwidth shift. Additionally, we use three guiding pins to mount the layers with the base plate. Also, the alignment process between the top and bottom mold, which is currently a manual process, can introduce about 20 to  $25 \mu\text{m}$  misalignment, which can affect the overall antenna performance. This misalignment could be a possible reason of the  $S_{11}$  peak around 145 GHz.

The radiation pattern and the gain of the array antenna were measured in an anechoic chamber. The simulated and measured radiation patterns are presented in Figs. 13, 14, and 15. Comparing the simulated radiation pattern with the measured radiation pattern, we see that the measured patterns show good agreement with the

**Fig. 13** Simulated and measured E-plane pattern and H-plane pattern at 132 GHz

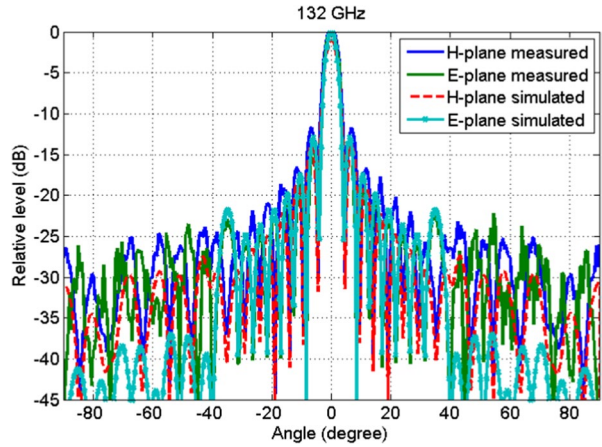


**Fig. 14** Simulated and measured E-plane pattern and H-plane pattern at 142 GHz

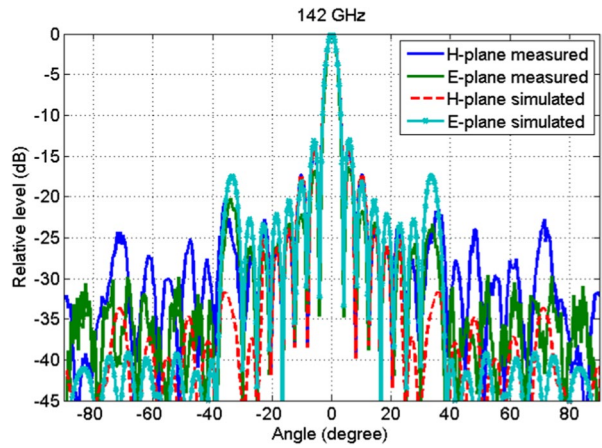
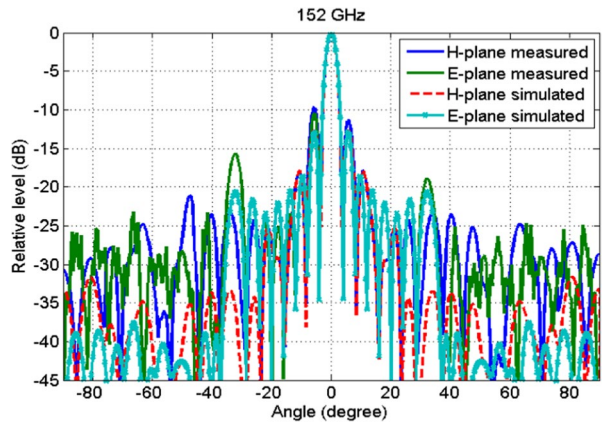


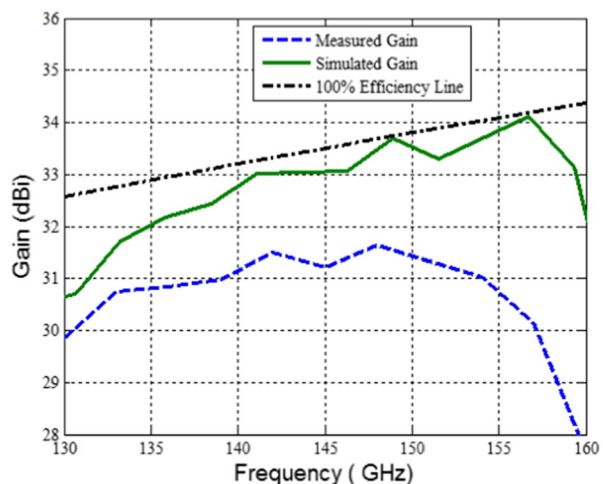
**Fig. 15** Simulated and measured E-plane pattern and H-plane pattern at 152 GHz



simulated patterns. The first side lobe is around  $-10$  dB, both in the E-plane and the H-plane which is a bit higher than the theoretical value of  $-13$  dB for a uniform array antenna. The far-out side lobes are  $-16$  dB lower in the E-plane and  $-20$  dB lower in the H-plane pattern, which also agrees well with the simulated values. Measured half power beam width (HPBW) for E-plane and H-plane are  $4.0^\circ$  and  $4.1^\circ$  at 132 GHz,  $3.7^\circ$  and  $3.9^\circ$  at 142 GHz, and  $3.6^\circ$  and  $3.8^\circ$  at 152 GHz, respectively. This implies that the fabrication process adopted in this work produces relatively low phase and amplitude imbalance within the  $16 \times 16$  array antenna. Otherwise, the measured side lobes of the antenna array would have relatively higher values.

The gain measurement result is presented in Fig. 16. The measured total gain is about 31 dBi over the band of interest from 135 to 150 GHz. The gain response is quite flat over the band of interest with a gain variation of approximately 1 dB. The maximum 2.25 dB difference between the simulated gain and measured gain occurs at the upper band edge, after 150 GHz. The measured total efficiency of the proposed antenna is calculated from the difference between the measured gain of the antenna and the maximum available directivity for the aperture size,  $D_{\max}$  (or the 100% efficiency line). It is found that the total efficiency of the antenna array varies between 53 and 62% over the frequency band 132–152 GHz and the efficiency is about 58% at mid band. There is a drop in gain after 152 GHz. The gain drop can be attributed to the following factors. One factor is due to the higher level of the reflected signal (higher value of  $S_{11}$  after 152 GHz). The second factor is that the side lobe of the antenna in the E-plane is around  $-15$  dB level at 152 GHz. This value is going to be higher above 152 GHz as the subarray size in the E-plane will become larger in terms of wavelength. Thus, power will be lost in these unwanted side lobes in the E-plane and this results in a decrease of main beam gain. The feed waveguide losses will also increase at higher frequency due to surface roughness; hence, the gain of the antenna deteriorates above 152 GHz. The measured surface roughness of the fabricated antenna is  $26 \text{ nm} \pm 8 \text{ nm}$ . In the simulation, the surface roughness was

**Fig. 16** Simulated and measured gain of the  $16 \times 16$  array



not considered. However, the measured total efficiency of the antenna is at least 53% over the band of interest, which is acceptable for the intended LOS-MIMO application. Also, it is believed that 10–15% BW is representative for LOS-MIMO backhaul link, as the regulatory studies on channel arrangements in Europe is going on, with the focus on the 92–114.25 GHz and 130–174.8 GHz ranges: commonly referred to as the W-band and D-band, respectively [35]. Therefore, the fabricated antenna with 14% BW will be suitable for LOS-MIMO application.

## 4.2 Comparison

This section provides a comparison of the performance of our antenna with similar 100-GHz frequency band antennas. The main structural features and performance of various reported 100 GHz high-gain antenna arrays are summarized in Table 2. Due to the lack of dielectric losses in the feed network, the proposed antenna has much higher efficiency compared to the ones presented in [10, 12]. The antenna efficiency of the proposed work is very similar to the hollow metal waveguide-based slot array antennas presented in [8]. It has been reported that the production cost can be reduced almost 60% by using injection molding process instead of CNC milling for batch fabrication of MEMS devices [36]. However, due to the relaxed fabrication requirements such as no requirement of electric connection between the side walls of gap waveguide technology, the production cost of the proposed antenna can be reduced by using polymer-based injection molding technique.

## 5 Conclusion

In this paper, we present a 140 GHz micromachined antenna array with more than 30-dBi gain which can be potentially used in a large 2D array for LOS-MIMO backhauling links. To develop a MIMO setup, it is important to consider the following parameters: antenna gain, working bandwidth of the antenna, form factor of the antenna, fabrication complexity, and production cost. We used different micromachining techniques to fabricate this antenna. The purpose of using a combined fabrication technique is to make the final fabrication process rapid and less complicated. The overall performance of the antenna elements consisting of three Au-coated polymer layers is satisfactory. The input reflection coefficient was measured to be below  $-11$  dB over a 14% bandwidth from 132 to 152 GHz, and the antenna gain was measured to be 31 dBi at 140 GHz, both of which are in good agreement with the simulations. Additionally, the performance of the polymer-based antenna array is expected to improve even further if we transfer this process towards a more automated fabrication method.

**Acknowledgements** The authors are grateful to the nanofabrication laboratory personnel at Chalmers University of Technology for their help with the fabrication process.

**Funding** This work has been supported by the innovation program “Smartare Elektroniksystem” by Vinova, Formas, and the Swedish Energy Agency the Wenner-Gren Foundation.

**Table 2** Comparison between the fabricated antenna and reported antenna works at 100 GHz

Ref	Fabrication method	Frequency (GHz)	Bandwidth – 10 dB $S_{11}$	Gain (dBi)	Efficiency (minimum)	Fabrication complexities vs antenna performance
[13]	CNC milling	94	21%	30	-	Time-consuming process, high production cost, good antenna performance
[8]	Diffusion bonding	120	13%	37	55%	High-temperature and high-pressure process, high production cost, high antenna efficiency
[9]	PolyStar process, micromach	150	3%	14	63%	High cost process, high antenna efficiency, narrow bandwidth
[12]	LTCC	140	22%	32	35%	Low-cost process, suffers from high dielectric losses, low antenna efficiency
[10]	Rogers PCB	94	6%	28.8	24%	Low-cost process but high dielectric losses, low antenna efficiency
[16, 37]	Silicon micromach	350	12%	29.5	50%	Time-consuming process, high-temperature and high-pressure process, high antenna efficiency
Our work	Polymer-based micro fabrication and injection molding	140	14%	31	53%	Low-cost process, once the mold is fabricated, the production is fast and suitable for batch production, high antenna efficiency

## Declarations

**Conflict of Interest** The authors declare no competing interests.

**Open Access** This article is licensed under a Creative Commons Attribution 4.0 International License, which permits use, sharing, adaptation, distribution and reproduction in any medium or format, as long as you give appropriate credit to the original author(s) and the source, provide a link to the Creative Commons licence, and indicate if changes were made. The images or other third party material in this article are included in the article's Creative Commons licence, unless indicated otherwise in a credit line to the material. If material is not included in the article's Creative Commons licence and your intended use is not permitted by statutory regulation or exceeds the permitted use, you will need to obtain permission directly from the copyright holder. To view a copy of this licence, visit <http://creativecommons.org/licenses/by/4.0/>.

## References

- [1] A. Hirata *et al.*, "120-GHz-Band Wireless Link Technologies for Outdoor 10-Gbit/s Data Transmission," *IEEE Transactions on Microwave Theory and Techniques*, vol. 60, no. 3, pp. 881–895, 2012.
- [2] K. Eriksson, P. J. Sobis, S. E. Gunnarsson, J. Hanning, and H. Zirath, "InP DHBT Amplifier Modules Operating Between 150–300 GHz Using Membrane Technology," *IEEE Transactions on Microwave Theory and Techniques*, vol. 63, no. 2, pp. 433–440, 2015.
- [3] X. Song and G. Fettweis, "On Spatial Multiplexing of Strong Line-of-Sight MIMO With 3D Antenna Arrangements," *IEEE Wireless Communications Letters*, vol. 4, no. 4, pp. 393–396, 2015.
- [4] F. Bohagen, P. Orten, and G. E. Oien, "Design of Optimal High-Rank Line-of-Sight MIMO Channels," *IEEE Transactions on Wireless Communications*, vol. 6, no. 4, pp. 1420–1425, 2007.
- Ericsson Press release. "Deutsche Telekom and Ericsson top 100Gbps over microwave link " <https://www.ericsson.com/en/press-releases/2019/5/deutsche-telekom-and-ericsson-top-100gbps-over-microwave-link> (accessed)
- [6] P. Zheng, G. Q. Zhao, S. H. Xu, F. Yang, and H. J. Sun, "Design of a W-Band Full-Polarization Monopulse Cassegrain Antenna," *IEEE Antennas and Wireless Propagation Letters*, vol. 16, pp. 99–103, 2017.
- [7] D. Kim, Y. Lim, H. Yoon, and S. Nam, "High-Efficiency W-Band Electroforming Slot Array Antenna," *IEEE Transactions on Antennas and Propagation*, vol. 63, no. 4, pp. 1854–1857, 2015.
- [8] D. Kim, J. Hirokawa, M. Ando, J. Takeuchi, and A. Hirata, "64 X 64-Element and 32 X 32-Element Slot Array Antennas Using Double-Layer Hollow-Waveguide Corporate-Feed in the 120 GHz Band," *IEEE Transactions on Antennas and Propagation*, vol. 62, no. 3, pp. 1507–1512, 2014.
- [9] E. D. Cullens, L. Ranzani, K. J. Vanhille, E. N. Grossman, N. Ehsan, and Z. Popovic, "Micro-Fabricated 130–180 GHz Frequency Scanning Waveguide Arrays," *IEEE Transactions on Antennas and Propagation*, vol. 60, no. 8, pp. 3647–3653, 2012.
- [10] Y. J. Cheng, Y. X. Guo, and Z. G. Liu, "W-Band Large-Scale High-Gain Planar Integrated Antenna Array," *IEEE Transactions on Antennas and Propagation*, vol. 62, no. 6, pp. 3370–3373, 2014.
- [11] B. Zhang, C. Kärfelt, H. Gulan, T. Zwick, and H. Zirath, "A D-Band Packaged Antenna on Organic Substrate With High Fault Tolerance for Mass Production," *IEEE Transactions on Components, Packaging and Manufacturing Technology*, vol. 6, no. 3, pp. 359–365, 2016.
- [12] Z. Miao *et al.*, "140 GHz High-Gain LTCC-Integrated Transmit-Array Antenna Using a Wide-band SIW Aperture-Coupling Phase Delay Structure," *IEEE Transactions on Antennas and Propagation*, vol. 66, no. 1, pp. 182–190, 2018.
- [13] A. Vosoogh, A. Haddadi, A. U. Zaman, J. Yang, H. Zirath, and A. A. Kishk, "W -Band Low-Profile Monopulse Slot Array Antenna Based on Gap Waveguide Corporate-Feed Network," *IEEE Transactions on Antennas and Propagation*, vol. 66, no. 12, pp. 6997–7009, 2018.

14. [14]Y. Wu, Z. Hao, Z. Miao, W. Hong, and J. Hong, "A 140 GHz High-Efficiency Slotted Waveguide Antenna Using a Low-Loss Feeding Network," *IEEE Antennas and Wireless Propagation Letters*, vol. 19, no. 1, pp. 94–98, 2020.
15. [15]X. Xu, M. Zhang, J. Hirokawa, and M. Ando, "E-Band Plate-Laminated Waveguide Filters and Their Integration Into a Corporate-Feed Slot Array Antenna With Diffusion Bonding Technology," *IEEE Transactions on Microwave Theory and Techniques*, vol. 64, no. 11, pp. 3592–3603, 2016.
16. [16]K. Tekkouk *et al.*, "Corporate-Feed Slotted Waveguide Array Antenna in the 350-GHz Band by Silicon Process," *IEEE Transactions on Antennas and Propagation*, vol. 65, no. 1, pp. 217–225, 2017.
17. [17]Y. Wang, M. Ke, M. J. Lancaster, and J. Chen, "Micromachined 300-GHz SU-8-Based Slotted Waveguide Antenna," *IEEE Antennas and Wireless Propagation Letters*, vol. 10, pp. 573–576, 2011.
18. [18]J. Liu, A. Vosoogh, A. U. Zaman, and J. Yang, "A Slot Array Antenna With Single-Layered Corporate-Feed Based on Ridge Gap Waveguide in the 60 GHz Band," *IEEE Transactions on Antennas and Propagation*, vol. 67, no. 3, pp. 1650–1658, 2019.
19. [19]A. Vosoogh, A. Haddadi, A. U. Zaman, J. Yang, H. Zirath, and A. A. Kishk, "W-Band Low-Profile Monopulse Slot Array Antenna Based on Gap Waveguide Corporate-Feed Network," *IEEE Transactions on Antennas and Propagation*, vol. 66, no. 12, pp. 6997–7009, 2018.
20. [20]E. Rajo-Iglesias, M. Ferrando-Rocher, and A. U. Zaman, "Gap Waveguide Technology for Millimeter-Wave Antenna Systems," *IEEE Communications Magazine*, vol. 56, no. 7, pp. 14–20, 2018.
21. [21]S. Rahiminejad *et al.*, "Micromachined ridge gap waveguide and resonator for millimeter-wave applications," *Sensors and Actuators A: Physical*, vol. 186, pp. 264–269, 2012/10/01/ 2012, doi: <https://doi.org/https://doi.org/10.1016/j.sna.2012.02.036>.
22. Rahiminejad S, Zaman AU, Haasl S, Kildal PS, Enoksson P, Demonstration of a micromachined planar distribution network in gap waveguide technology for a linear slot array antenna at 100 GHz, *Journal of Micromechanics and Microengineering*, vol. 26, no. 7, p. 074001, 2016/05/20 2016
23. Farjana S *et al* "Polymer based 140 GHz Planar Gap Waveguide Array Antenna for Line of Sight (LOS) MIMO Backhaul Links," presented at the IEEE MTT-S International Microwave Workshop Series on Advanced Materials and Processes, Bochum, Germany, July 16–18, 2019
24. [24]G. Pardon *et al.*, "Rapid mold-free manufacturing of microfluidic devices with robust and spatially directed surface modifications," *Microfluidics and Nanofluidics*, journal article vol. 17, no. 4, pp. 773–779, October 01 2014.
25. Zaman AU and Kildal PS (2016) "GAP Waveguides," in *Handbook of Antenna Technologies*, Chen ZN, Liu D, Nakano H, Qing X, Zwick T Eds. Singapore: Springer Singapore, pp. 3273–3347
26. [26]A. Farahbakhsh, D. Zarifi, and A. U. Zaman, "A mmWave Wideband Slot Array Antenna Based on Ridge Gap Waveguide With 30% Bandwidth," *IEEE Transactions on Antennas and Propagation*, vol. 66, no. 2, pp. 1008–1013, 2018.
27. [27]D. Zarifi, A. Farahbakhsh, A. U. Zaman, and P. Kildal, "Design and Fabrication of a High-Gain 60-GHz Corrugated Slot Antenna Array With Ridge Gap Waveguide Distribution Layer," *IEEE Transactions on Antennas and Propagation*, vol. 64, no. 7, pp. 2905–2913, 2016.
28. [28]E. Rajo-Iglesias and P. Kildal, "Numerical studies of bandwidth of parallel-plate cut-off realised by a bed of nails, corrugations and mushroom-type electromagnetic bandgap for use in gap waveguides," *IET Microwaves, Antennas & Propagation*, vol. 5, no. 3, pp. 282–289, 2011.
29. [29]A. d. Campo and C. Greiner, "SU-8: a photoresist for high-aspect-ratio and 3D submicron lithography," *Journal of Micromechanics and Microengineering*, vol. 17, no. 6, pp. R81–R95, 2007/05/15 2007.
30. [30]S. Rahiminejad, E. Pucci, S. Haasl, and P. Enoksson, "SU8 ridge-gap waveguide resonator," *International Journal of Microwave and Wireless Technologies*, vol. 6, no. 5, pp. 459–465, 2014.
31. [31]S. Rahiminejad, E. Pucci, V. Vassilev, P. Kildal, S. Haasl, and P. Enoksson, "Polymer Gap Adapter for Contactless, Robust, and Fast Measurements at 220–325 GHz," *Journal of Microelectromechanical Systems*, vol. 25, no. 1, pp. 160–169, 2016.
32. [32]S. W. Lee and S. S. Lee, "Shrinkage ratio of PDMS and its alignment method for the wafer level process," *Microsystem Technologies*, journal article vol. 14, no. 2, pp. 205–208, February 01 2008.
33. Madsen MH, Feidenhansl NA, Hansen P-E, Garnæs J, Dirscherl K Accounting for PDMS shrinkage when replicating structures *Journal of Micromechanics and Microengineering*, vol. 24, no. 12, p. 127002, 2014/10/29 2014
34. Y. X., Whitesides GM SOFT LITHOGRAPHY *Annual Review of Materials Science*, vol. 28, no. 1, pp. 153–184, 1998



35. CEPT ECC WG SE19, Work items SE19\_37 and SE19\_38, available at the following link <http://eccwp.cept.org/default.aspx?groupid=45>
36. Silverio, Vania & Cardoso, Susana. (2018). Microfabrication Techniques for Microfluidic Devices. [https://doi.org/10.1007/978-3-319-59593-1\\_2](https://doi.org/10.1007/978-3-319-59593-1_2)
37. Tekkoui K et al Plate-laminated corporate-feed slotted waveguide array antenna at 350-GHz band by silicon process in 2016 International Symposium on Antennas and Propagation (ISAP), 24–28 Oct. 2016 2016, pp. 538–539

**Publisher's Note** Springer Nature remains neutral with regard to jurisdictional claims in published maps and institutional affiliations.

## Authors and Affiliations

**Sadia Farjana**<sup>1</sup>  · **Mohammad Amir Ghaderi**<sup>1</sup> · **Ashraf Uz Zaman**<sup>2</sup> · **Sofia Rahiminejad**<sup>3</sup> · **Thomas Eriksson**<sup>2</sup> · **Jonas Hansson**<sup>4</sup> · **Yinggang Li**<sup>5</sup> · **Thomas Emanuelsson**<sup>6</sup> · **Sjoerd Haas**<sup>7</sup> · **Per Lundgren**<sup>1</sup> · **Peter Enoksson**<sup>1</sup>

<sup>1</sup> Department of Microtechnology and Nanoscience, Chalmers University of Technology, Gothenburg, Sweden

<sup>2</sup> Department of Electrical Engineering, Chalmers University of Technology, Gothenburg, Sweden

<sup>3</sup> Nasa Jet Propulsion Laboratory, Pasadena, CA, USA

<sup>4</sup> Mercene Labs AB, Stockholm, Sweden

<sup>5</sup> Ericsson AB, Gothenburg, Sweden

<sup>6</sup> Gapwaves AB, Gothenburg, Sweden

<sup>7</sup> RISE Research Institutes of Sweden AB, Stockholm, Sweden